THE JOURNAL OF BIOLOGICAL CHEMISTRY
Vol. 278, No. 9, Issue of February 28, pp. 7199–7205, 2003

Printed in U.S.A.

Low Resolution Structure Determination Shows Procollagen C-Proteinase Enhancer to be an Elongated Multidomain Glycoprotein*

Received for publication, October 23, 2002, and in revised form, December 10, 2002
Published, JBC Papers in Press, December 15, 2002, DOI 10.1074/jbc.M210857200

Simonetta Bernocco‡§, Barry M. Steiglitz¶, Dmitri I. Svergun‖, Maxim V. Petoukhov‖**, Florence Ruggiero‡, Sylvie Ricard-Blum‡‡, Christine Ebel‡‡, Christophe Geourjon‡, Gilbert Deléage‡, Bernard Font‡, Denise Eichenberger‡, Daniel S. Greenspan¶, and David J. S. Hulmes‡§§**

*From the ‡Institut de Biologie et Chimie des Protéines, UMR 5086 CNRS-UCBL1, 69367 Lyon cedex 07, France, the ¶Departments of Pathology and Biomolecular Chemistry, University of Wisconsin, Madison, Wisconsin 53706, the ‖European Molecular Biology Laboratory, Hamburg Outstation, 22603 Hamburg, Germany, the **Institute of Crystallography, Russian Academy of Sciences, 117333 Moscow, Russia, and the ‡‡Institut de Biologie Structurale, UMR 5075 CEA-CNRS-UJF, 38027 Grenoble cedex 1, France*

Procollagen C-proteinase enhancer (PCPE) is an extracellular matrix glycoprotein that can stimulate the action of tolloid metalloproteinases, such as bone morphogenetic protein-1, on a procollagen substrate, by up to 20-fold. The PCPE molecule consists of two CUB domains followed by a C-terminal NTR (netrin-like) domain. In order to obtain structural insights into the function of PCPE, the recombinant protein was characterized by a range of biophysical techniques, including analytical ultracentrifugation, transmission electron microscopy, and small angle x-ray scattering. All three approaches showed PCPE to be a rod-like molecule, with a length of ~150 Å. Homology modeling of both CUB domains and the NTR domain was consistent with the low-resolution structure of PCPE deduced from the small angle x-ray scattering data. Comparison with the low-resolution structure of the procollagen C-terminal region supports a recently proposed model (Ricard-Blum, S., Bernocco, S., Font, B., Moali, C., Eichenberger, D., Farjanel, J., Burchardt, E. R., van der Rest, M., Kessler, E., and Hulmes, D. J. S. (2002) *J. Biol. Chem.* 277, 33864–33869) for the mechanism of action of PCPE.

Most extracellular matrix proteins are modular in structure (1, 2), including procollagen C-proteinase enhancer (PCPE,[1] molecular mass ~50 kDa), which consists of two CUB domains followed by a C-terminal NTR domain (3, 4). One function of PCPE is to enhance the activities of tolloid metalloproteinases (BMP-1, mTLD) (5–7), during procollagen processing, by up to 20-fold (8–10). Tolloid metalloproteinases are involved in a variety of morphogenetic events such as processing of procollagens (11–15) (leading to fibril assembly) and prolysyl oxidases (16, 17) (initiating covalent cross-linking in collagens and elastin). They also cleave probiglycan (18), laminin 5 (19, 20) (affecting keratinocyte adhesion/migration, Ref. 21) and chordin/SOG (22, 23) (controlling dorso-ventral patterning). Enhancement of tolloid proteinase activity, on a procollagen I substrate, by PCPE has been shown to be a property of the CUB domain region (3, 9, 10). Possible roles of PCPE in tolloid proteinase processing of non-procollagen substrates are unknown.

CUB domains are found exclusively in extracellular and plasma membrane-associated proteins. In addition to PCPE and the recently discovered PCPE2 (24), these include the tolloid metalloproteinases BMP-1/mTLD, mTLL-1, and mTLL-2 (6, 7, 23), the metalloproteinase ADAMTS13 (25), the complement serine proteinases C1r, C1s, MASP1, MASP2, and MASP3 (26, 27) and the membrane serine proteinases enteropeptidase/enterokinase (28) and matriptases-1 and -2 (29, 30). Further extracellular proteins include the spermadhesins (31), proteins consisting of single CUB domains involved in mammalian fertilization, the inflammation-associated protein TSG-6 (32), the growth factor PDGF-C/fallotein (33), and salivary agglutinin/gp-340/DMBT1 (34). Attractin, which exists in both secreted and membrane-bound forms, displays dipeptidyl peptidase activity and is involved in T cell clustering, skin pigmentation, and the control of energy metabolism (35). Further membrane-associated proteins include cubulin (36), a multi-CUB domain protein involved in intestinal absorption of cobalamin (vitamin B_{12}) as well as renal protein re-absorption, and the neuropilins (37), involved in axonal guidance and angiogenesis.

A number of roles for CUB domains have been assigned in protein-protein and protein-carbohydrate interactions. In PCPE, the CUB domains bind to the C-propeptide region of fibrillar procollagens (9), as well as elsewhere in the procolla-

* This work was supported by the CNRS (Programme Protéomique et Génie des Protéines), the Université Claude Bernard Lyon 1, the Commissariat à l'Energie Atomique, the Association pour la Recherche sur le Cancer, the European Community (Access to Research Infrastructure Action of the Improving Human Potential Programme, Grant HPRI-CT-1999-00017 (to the EMBL Hamburg Outstation); Grant QLK3-2000-00084 (to F. R.)), the International Association for the Promotion of Cooperation with Scientists from the Independent States of the Former Soviet Union, Grants 00-243 and YSF 00-50 (to D. I. S. and M. V. P.), and the National Institutes of Health (Predoctoral Training Grant T32 GM07215 (to B. M. S.) and Grants AR47746 and GM63471 (to D. S. G.)). The costs of publication of this article were defrayed in part by the payment of page charges. This article must therefore be hereby marked "*advertisement*" in accordance with 18 U.S.C. Section 1734 solely to indicate this fact.

§ Present address: Sienabiotech, Via Fiorentina 1, 53100 Siena, Italy.
§§ To whom correspondence should be addressed: Institut de Biologie et Chimie des Protéines, CNRS UMR 5086, 7, passage du Vercors, 69367 Lyon Cedex 07, France. Tel.: 33-0-4-72-72-26-67; Fax: 33-0-4-72-72-26-04; E-mail: d.hulmes@ibcp.fr.

[1] The abbreviations used are: PCPE, PCP enhancer; PCP, procollagen C-proteinase; BMP-1, bone morphogenetic protein-1; CUB, module found in complement subcomponents Clr/Cls, Uegf, and BMP-1; mTLD, mammalian tolloid; mTLL, mammalian tolloid-like; NTR, netrin-like; SAXS, small angle X-ray scattering; TIMP, tissue inhibitor of metalloproteinases.

gen molecule (38). In C1r and C1s, CUB domains are required for C1s-C1r-C1r-C1s tetramer formation as well as interaction of the tetramer with the collagen-like regions of C1q (27). Similar roles have been demonstrated for the CUB domains of MASP-1 and MASP-2 (as well as its alternatively spliced form Map19), in homodimer formation and binding to the collagen-like region of mannan binding lectin (39, 40). Some spermadhesins display carbohydrate binding activity (31). In cubulin, CUB domains are involved in binding to albumin and to the intrinsic factor-cobalamin complex (36), while in neuropilin-1 CUB domains are required for binding to semaphorin 3A (37).

The NTR module (4) occurs solely in extracellular proteins, whose functions are sometimes similar or complementary to those of CUB-containing proteins. The NTR family includes the netrins (41) (proteins involved in axonal guidance), complement proteins C3, C4, and C5 (26), secreted frizzled-related proteins (42) (mediators of Wnt signaling), WFIKKN (43) (a protein containing multiple protease-inhibitory modules) and TIMPs (44). Possible functions for NTR domains are based on their homologies with the N-terminal active domain of TIMPs. In the case of PCPE, it has recently been shown that fragments corresponding to the free NTR domain are present in the conditioned medium of human brain tumor cells, where they appear to have moderate TIMP-like activity (45). While it has been speculated (4, 42, 43) that other NTR-containing proteins might also show TIMP-like activity, direct experimental evidence for this is lacking. Nevertheless, the possibility that PCPE contains domains that can either enhance (CUB) or inhibit (NTR) different metalloproteinases is intriguing. A further possibility is that the NTR and/or CUB domains in PCPE are involved in the observed effects of this protein on the control of cell growth (46–48), as has also been observed for TIMPs, independent of metalloproteinase inhibitory activity (44).

So far the only CUB-containing proteins for which high resolution three-dimensional structures have been determined are the spermadhesins (31). While this has permitted the molecular modeling of individual CUB domains in various proteins (32, 37, 49, 50), there exists at present no information on how contiguous CUB domains might be arranged in three dimensions. High-resolution structures of TIMPs (51, 52) permit molecular modeling of the NTR domain. Here we use a variety of biophysical techniques, together with molecular modeling, to determine the low-resolution structure of PCPE. We show that the molecule is highly elongated, and this gives insights into how PCPE enhances procollagen C-proteinase activity.

EXPERIMENTAL PROCEDURES

Expression and Purification of Recombinant PCPE—The 1474-bp cDNA clone KT11 (3) was used as the template for PCR amplification of sequences corresponding to full-length human PCPE, minus signal peptide sequences, using forward primer 5′-ACTGTCAGCTAGCACAGACCCCCAACTACACCAGACCC-3′ and reverse primer 5′-GCATGCGGCCGCAGTCCTGGGACGCAGCAG-3′, which contained a *Nhe*I or *Not*I site, respectively, to facilitate subsequent cloning steps. The ~1.3-kb PCR product was ligated into pGEM-T, sequenced fully on both strands to ensure an error-free clone, excised by digestion with *Nhe*I and *Not*I and ligated in-frame between the *Nhe*I and *Not*I sites of the vector pCEP-Pu/BM40s (53). Excision of fused BM40-PCPE sequences from the latter construct with *Kpn*I and *Not*I and insertion between the *Kpn*I and *Not*I sites of expression vector pcDNA3.1 (Invitrogen) yielded a construct designed to produce a translation product differing from native PCPE only in the replacement of the native signal peptide by the BM40 signal sequence (for enhancement of secretion). Proper insertion of sequences was verified by DNA sequencing of insert-vector junctions.

Human 293 embryonic kidney cells, purchased from the American Type Culture Collection (Manassas, VA) and maintained in growth medium consisting of Dulbecco's modified Eagle's medium (DMEM)/10% fetal bovine serum (14), were transfected with the PCPE/pcDNA3.1 expression vector, using LipofectAMINE, according to the manufacturer's protocols (Invitrogen). Two days post-transfection, cells were placed in growth medium containing 500 μg/ml G418 (Invitrogen), selected for approximately 2 weeks, then G418-resistant clonal lines were picked with cloning cylinders and maintained in growth medium containing 250 μg/ml G418. Confluent monolayers of the clonal line determined by Western blotting to produce the highest levels of recombinant PCPE (rPCPE) were washed three times with phosphate-buffered saline and incubated in Dulbecco's modified Eagle's medium containing 250 μg/ml G418 and 40 μg/ml soybean trypsin inhibitor (Sigma) for 24 h. Medium was harvested and centrifuged to remove cell debris, and protease inhibitors were added to final concentrations of 10 mM EDTA, 1 mM 4-aminobenzamidine dihydrochloride, 1 mM *N*-ethylmaleimide, and 0.5 mM phenylmethylsulfonyl fluoride. Conditioned medium, which was typically found to contain ~15 μg/ml PCPE, was stored at −70 °C until further use.

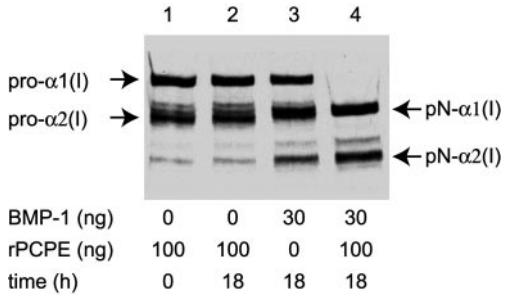

FIG. 1. **Recombinant PCPE enhances type I procollagen processing *in vitro*.** Fluorograms are shown of radiolabeled type I procollagen incubated in the presence or absence of purified rPCPE and/or BMP-1 for the indicated times. Pro-α1(I) and pro-α2(I) procollagen chains and pN-α1(I) and pN-α2(I) processing intermediates generated by BMP-1 activity are indicated by *arrows*.

Recombinant PCPE from conditioned 293 cell media was purified as described (54) for rPCPE produced in a baculovirus system. The purified protein, in 20 mM Hepes, 300 mM NaCl pH 7.4, was then concentrated and buffer exchanged, to up to 30 mg/ml in 20 mM Hepes, 150 mM NaCl pH 7.4, using UltraFree 15 microconcentrators (Millipore, 10 kDa cut-off), and stored at −80 °C.

Assay of Enhancing Activity—Human ^{3}H-labeled type I procollagen and recombinant BMP-1 with a C-terminal FLAG epitope were prepared and purified as previously described (23). Procollagen substrate (400 ng) was incubated at 37 °C either alone or in combination with 100 ng purified rPCPE and/or 30 ng BMP-1 in 20 μl of 50 mM Tris-HCl, pH 7.5, 150 mM NaCl, 5 mM $CaCl_2$. Following incubation for the indicated period, reactions were stopped by the addition of 10× concentrated SDS-PAGE sample buffer containing 2-mercaptoethanol and boiling for 5 min. Following electrophoresis, processing intermediates were visualized as previously described (23).

Mass Spectrometry—Mass spectrometry analysis was performed on an Applied Biosystems MALDI-TOF Voyager DE-PRO mass spectrometer operating in delayed extraction and linear mode. The rPCPE sample was analyzed after dialysis against 0.1 M ammonium acetate and purification using a ZipTip^{TM} C_4 (Millipore). The matrix was a saturated solution of sinapinic acid (5 mg) in 0.5 ml of 30% (v/v) CH_3CN, 0.1% trifluoroacetic acid.

Analytical Ultracentrifugation—Sedimentation velocity experiments were performed using a Beckman XL-I analytical ultracentrifuge and an AN-60 TI rotor. Experiments were carried out at 20 °C in 10 mM Hepes, 150 mM NaCl, pH 7.4. Two samples of 400 μl at protein concentrations of 0.4 and 1.2 mg/ml were loaded into 12-mm path cells and centrifuged at 42,000 rpm. Scans were recorded at 277 nm every 5 min using a 0.03-mm radial spacing.

Sedimentation profiles were analyzed using SEDFIT (55) (www.analyticalultracentrifugation.com), which takes advantage of a radial and time-independent noise subtraction procedure (56), to directly model boundary profiles in terms of a continuous distribution of discrete species and of non-interacting components. This allows the evaluation of both sedimentation (s) and diffusion (D) coefficients, from which the molar mass is derived using the Svedberg equation: $M = s\,RT/D(1 - \rho\bar{\nu})$. We estimated the partial specific volume ($\bar{\nu}$) of rPCPE, from its amino acid composition (assuming an additional molecular mass of ~3 kDa due to glycosylation equivalent to 17 hexose units per PCPE molecule) to be 0.721 ml/g, the solvent density ρ to be 1.005 g/ml, and the solvent viscosity η to be 1.002 mPa·s, at 20 °C using SEDNTERP software (V1.01; developed by D. B. Haynes, T. Laue, and J. Philo,

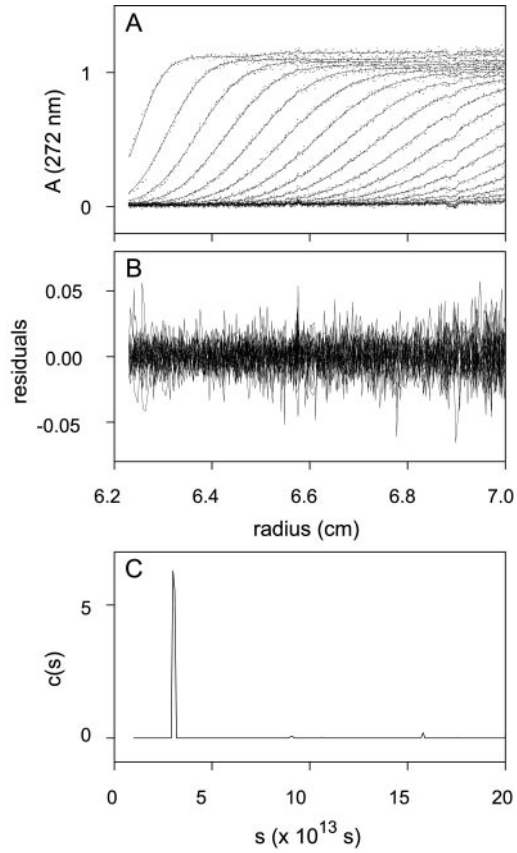

FIG. 2. **Analytical ultracentrifugation of rPCPE.** *A*, snapshots of absorbance as a function of time and distance from the axis of rotation, showing experimental values (*dots*) and theoretical fits (*lines*). *B*, residuals showing differences between observed and theoretical curves. *C*, distribution of particles according to their sedimentation coefficients.

www.bbri.org/RASMB/rasmb.html), which was also used for the calculation of the corrected $s_{20,w}$ and $D_{20,w}$ values, and calculated minimum values of the hydrodynamic diameter D_h.

Rotary Shadowing—Purified rPCPE was dialyzed against 0.1 M ammonium acetate. Samples were then diluted in the same buffer and mixed with glycerol (1:1) to obtain final concentrations of rPCPE ranging from 5 to 15 μg/ml. A drop of the solution was then placed onto freshly cleaved mica sheets, using the "mica sandwich" technique (57) and immediately transferred to the holder of a MED 010 evaporator (Balzers). Rotary shadowing was carried out by evaporating platinum at an angle of 8°, followed by evaporation of carbon at 90°. Replicas were floated onto distilled water, picked up on copper grids and examined with a Philips CM120 microscope at the "Centre Technologique des Microstructures" (Université Claude Bernard, Lyon I).

Small Angle X-ray Scattering—Synchrotron radiation x-ray scattering data were collected using standard procedures on the X33 camera (58–60) at the European Molecular Biology Laboratory (EMBL) Hamburg Outstation on storage ring DORIS III of the Deutsches Elektronen Synchrotron (DESY), using multiwire proportional chambers with delay line readout (61). Samples were measured at protein concentrations of 3.1, 4.6, and 30.8 mg/ml, determined by absorbance at 280 nm using an absorbance of 0.8 at 1 mg/ml calculated from the amino acid sequence. Scattering curves were recorded at a wavelength (λ) of 1.5 Å at a sample-detector distance of 1.8 m covering the momentum transfer range $0.015 < s < 0.43$ Å^{-1} ($s = 4\pi\sin\theta/\lambda$, where 2θ is the scattering angle).

Data were normalized to the intensity of the incident beam and corrected for detector response, the scattering of buffer was subtracted, and the difference curves were scaled for concentration using the program PRIMUS.[2] To check for radiation damage and aggregation during the small angle x-ray scattering (SAXS) experiment, the data were collected in 10 successive 1-min frames. Reduced data sets at low angles were then extrapolated to zero concentration following standard procedures (62) and then merged with the higher angle data to yield the final composite scattering curves.

To eliminate scattering from a minor population of high molecular mass aggregates (which appeared possibly as a result of freezing and/or concentrating the sample) rPCPE in the low concentration range (3–5 mg/ml) was analyzed directly after further purification by gel permeation chromatography on Superdex 200, using 20 mM Hepes, 500 mM NaCl, pH 7.4 as elution buffer. Data from these samples were used for the very low angle region while higher angle data were obtained with rPCPE purified using the standard protocol (see above) then adjusted to 500 mM NaCl and centrifuged for 15 min at 17,500 × *g*.

The molar mass of rPCPE in solution was calculated by SAXS by comparing the forward scattering with that from freshly made reference solutions of bovine serum albumin (molar mass = 66 kDa). The

[2] P. V. Konarev, V. V. Volkov, M. H. J. Koch, and D. I. Svergun, submitted manuscript.

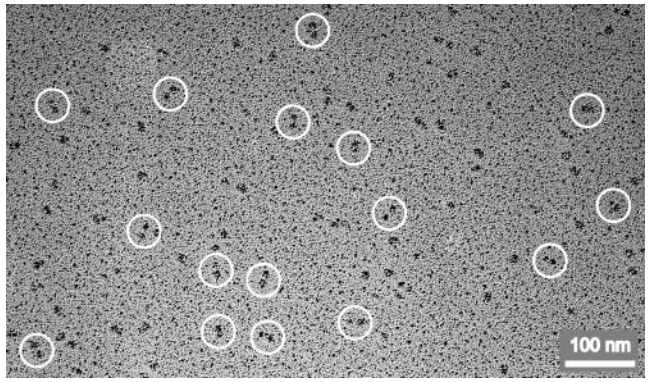

FIG. 3. **Transmission electron microscopy of rPCPE after rotary shadowing.** Molecules are either globular in shape or rod-like consisting of two closely adjacent lobes (*circled*).

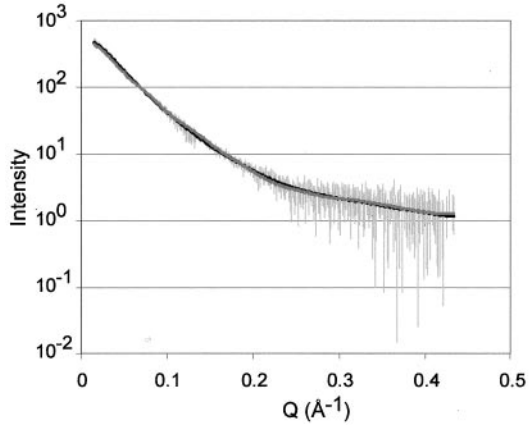

FIG. 4. **Small angle x-ray scattering curve of rPCPE in solution.** Experimental data (with *error bars*) are shown as a function of *s* (see "Experimental Procedures"), in comparison with a typical theoretical fit, obtained here with GASBOR (*black line*). Fits with DAMMIN and DALAI_GA were equally good (not shown). Also shown (*gray line*) is the best fit curve generated with CREDO corresponding to one of the structures shown in Fig. 8, including modeled CUB and NTR domains as well as terminal and linker regions.

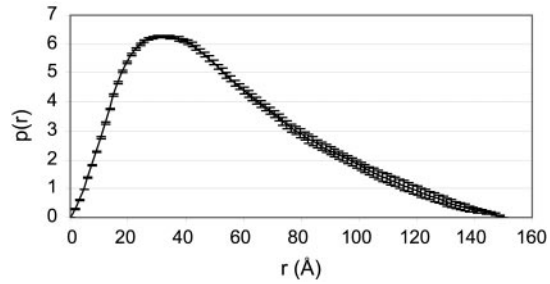

FIG. 5. **Pair distribution function calculated for rPCPE from the SAXS data.** The *curve* shows the distribution of interatomic spacings in rPCPE, with a maximum at 150 Å.

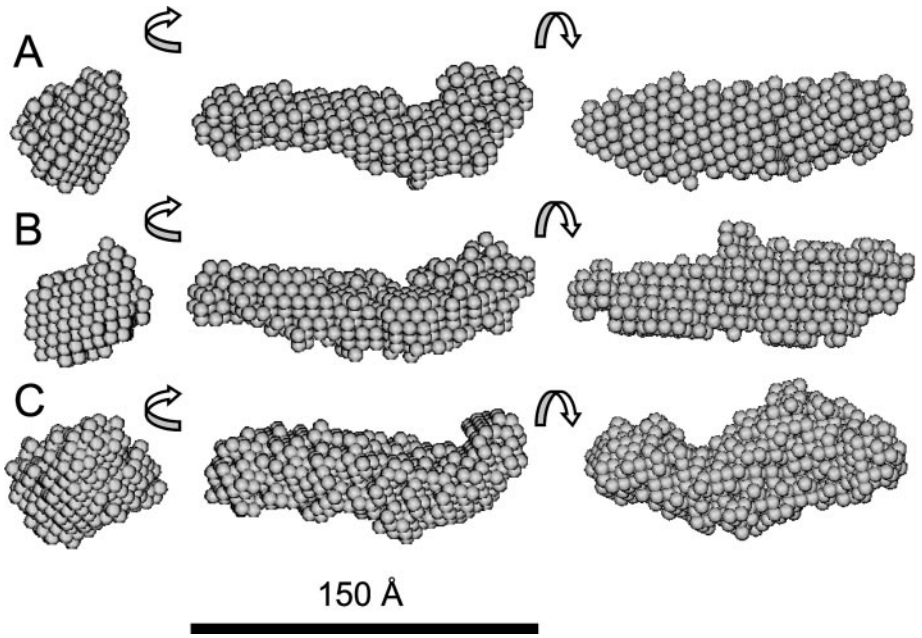

FIG. 6. **Structures generated *ab initio* from the SAXS data.** Molecular shapes are represented in projection, from three orthogonal directions, by arrays of beads, generated using the programs DAMMIN (*A*), DALAI_GA (*B*), and GASBOR (*C*). For each structure, the results of at least ten independent simulations were averaged. Orientations with respect to the views shown in the central column (in which the pointed and blunt ends are to the *left* and *right*, respectively) are indicated by *curved arrows*. Structures were aligned using DAMAVER and displayed using ASSA (76).

radius of gyration R_g was evaluated using the Guinier approximation, $I_{exp}(s) = I(0)\exp(-s^2R_g^2/3)$, which is valid for $(sR_g) < 1.3$ (62), and also from the entire scattering curve using with the indirect transform package GNOM (63). GNOM was also used to evaluate the forward scattering $I(0)$ and distance distribution function $p(r)$. The maximum dimension D_{max} was also estimated using the orthogonal expansion program ORTOGNOM (64).

Low resolution models of the protein were generated *ab initio* using the programs DAMMIN (slow mode) (65), DALAI_GA (66), and GASBOR (67), using the smoothed data set generated by GNOM. Both DAMMIN and DALAI_GA represent the particle as a collection of $M \gg 1$ densely packed beads inside the search volume (a sphere with diameter D_{max}). Each bead belongs either to the particle or to the solvent, and the shape is thus described by a binary string of length M. Starting from a random string, simulated annealing (DAMMIN) or the genetic algorithm (DALAI_GA) is employed to search for a compact model that fits the data, after subtracting a small constant from each data point to force the s^{-4} decay of the intensity at higher angles (65, 66). Modeling using DALAI_GA was carried out using cycles with progressively smaller beads starting at a radius of 8.5 decreasing to 3.5 Å in steps of 1 Å. The program GASBOR represents a protein by an assembly of dummy residues (DRs) and uses simulated annealing to build a locally "chain-compatible" DR-model inside the same search volume. The DR modeling is able to fit higher resolution data (without subtraction of a constant) and generally provides more detailed models than those given by the shape determination algorithms. With each program, final models were obtained by averaging at least ten independent runs using the program DAMAVER.[3]

Molecular Modeling—Models were built by homology for the CUB1, CUB2 and NTR domains with the help of the program Geno3D (68). This approach first extracts homology-derived spatial constraints on many atom-atom distances and dihedral angles from the template structure(s). An alignment is used to determine equivalent residues between the target and the template. The homology-derived and stereochemical constraints are then used to generate protein models that best satisfy these criteria. CUB1 (residues 37–146, numbered from the start of translation) and CUB2 (residues 159–275) domains were modeled using the acidic seminal fluid protein structure (PDB code: 1SFP) as the template (31), while the template for the NTR module (residues 318–437) was the structure of TIMP-2 (PDB code: 1BR9) (51).

Models were fitted by eye to the structures derived from small angle x-ray scattering using the program MASSHA (69). The program CRYSOL (70) was then used to calculate the theoretical SAXS profile based on this three-dimensional arrangement of domains. The program suite CREDO (71) was used to model the missing portions of the structure corresponding to the N and C termini (residues 26–36 and 438–449, respectively, assuming residues 1–25 to represent the signal sequence)

[3] V. V. Volkov and D. I. Svergun, submitted manuscript.

```
                                   CUB1
1SFP        CGGILKEESGVIAT-----YYGPKTNCVWTIQMPPEYHVRVSIQYLQL----NCNKESLE
PCPE_CUB1   CGGDVKGESGYVASEGFPNLYPPNKECIWTITVPEGQTVSLSFRVFDLELHPACRYDALE
            *** * *** *       * *   * *** *     *   *   *     *    **

1SFP        IIDG-LPGSPVLGKIC-EGSLMDYRSSGSIMTVKYIREPEHPASFYEVLY
PCPE_CUB1   VFAGSGTSGQRLGRFCGTFRPAPLVAPGNQVTLRMTTDEGTGGRGFLLWY
              *        **  *          *   *              *

                                   CUB2
1SFP        CGGILKEESGVI-----ATYYGPKTNCVWTIQMPPEYHVRVSIQYLQL----NCNKESL
PCPE_CUB2   CGGRLEKAQGTLTTPNWPESDYPPGISCSWHIIAPPDQVIALTFEKFDLEPDTYCRYDSV
            *** *    *           * *   * * *  **           *     *   *

1SFP        EIIDGLPG--SPVLGKIC-EGSLMDYRSSGSIMTVKYIREPEHPASFYEVLYFQDPQ
PCPE_CUB2   SVFNGAVSDDSRRLGKFCGDAVPGSISSEGNELLVQFVSDLSVTADGFSASYKTLPR
              *    *  *** *          * *   *         *     *   *

                                   NTR
1BR9        CS--CSPVH-PQQAFCNADVVIRAKAVSEKEVDSGNDIYGNPIKRIQYEIKQIKMFKGPE
PCPE_NTR    CPKQCRRTGTLQSNFCASSLVVTATVKSMVREPGE---------GLAVTVSLIGAYKTGG
            *   *       *  **    *   *   *                     *   *

1BR9        KD------IEFIYTAPSSAVCG-VSLDVGGKKEYLIAGKAEGDGKMHITLCDFIVPWDTL
PCPE_NTR    LDLPSPPTGASLKFY---VPCKQCPPMKK-GVSYLLMGQVEENRGPVLPPESFVVLHR--
             *                 *            **  *  *           * *

1BR9        STTQKKSLNHRYQMGC
PCPE_NTR    -PNQDQILTNLSKRKC
              *   *       *
```

FIG. 7. **Sequence alignments of PCPE CUB and NTR domains.** CUB domain sequences are aligned with that of the acidic seminal fluid protein (PDB code: 1SFP) while the NTR sequence is aligned with that of TIMP-2 (PDB code: 1BR9). Identical residues (*in bold*) are indicated by *asterisks*.

and the CUB1-CUB2 and CUB2-NTR linker regions (residues 147–158 and 276–317, respectively).

RESULTS

Protein Production and Characterization—In order to produce sufficient quantities of PCPE for structural analyses, transfected 293 human embryonic kidney cells were employed to establish a clonal cell line that constitutively produced ~15 μg rPCPE per ml of conditioned medium. As seen in Fig. 1, although rPCPE had no intrinsic procollagen C-proteinase activity (*lanes 1* and *2*), it stimulated BMP-1-mediated processing of type I procollagen to completion under the assay conditions (*lanes 3* and *4*). Thus, the rPCPE has procollagen C-proteinase enhancing activity indicative of a native conformation suitable for structural analysis.

Analytical Ultracentrifugation—When subjected to analytical ultracentrifugation, rPCPE was found to sediment essentially as a single, slowly sedimenting population with a minor, faster moving component (Fig. 2). When fitted using a two

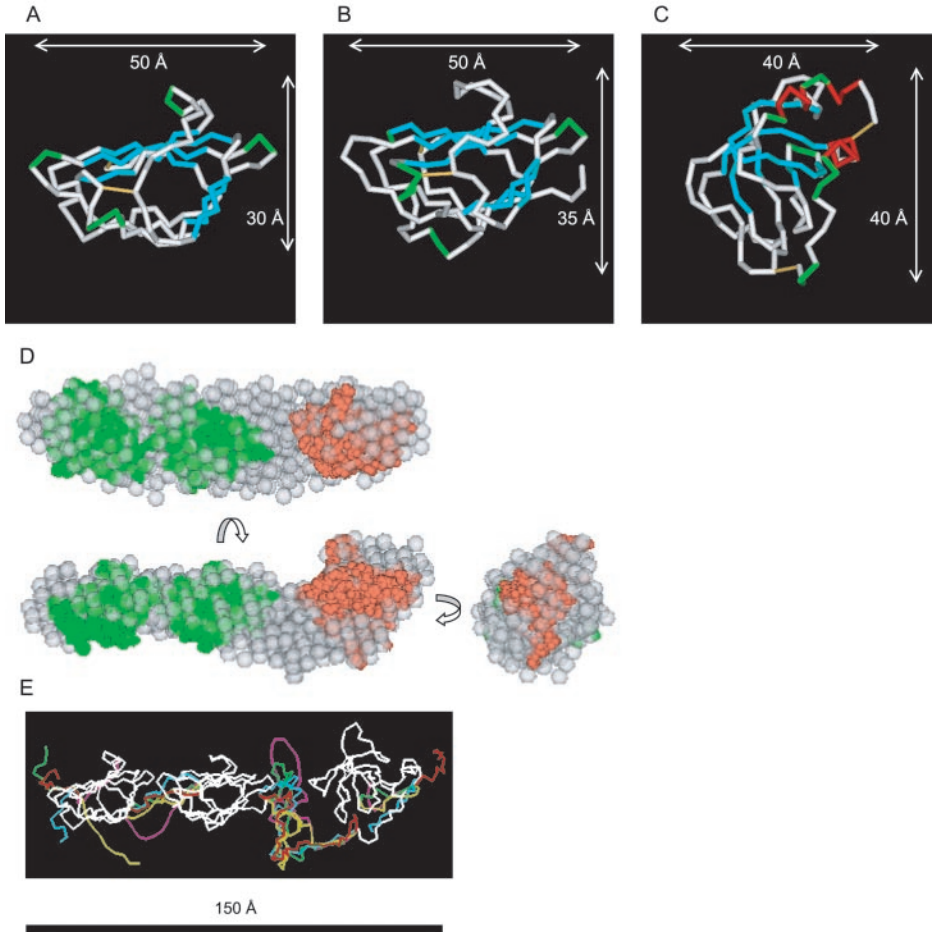

FIG. 8. **Three-dimensional models for rPCPE and its domains.** *A*, CUB1; *B,* CUB2; and *C,* NTR. α-helical residues are in *red*, β-sheets in *blue*, turns in *green*, and remaining structures in *white*. Disulfide bridges are in *yellow*. Dimensions are calculated from the maximum lengths in projection. Models are displayed as α-carbon traces using VIEWERLITE (Accelrys). *D*, superposition of structures shown in *A*, *B*, and *C* with the averaged structure generated by DAMMIN from the SAXS data. Three orthogonal views are shown, represented by beads, with the DAMMIN structure in semi-transparent gray, the CUB domains in *green* and the NTR domain in *orange*. Structures displayed using ASSA (76). *E*, three-dimensional structures of terminal and linker regions generated using CREDO in five independent runs (shown in *color*), together with the domain arrangement from *D* shown in *white* (same scale and same orientation as in *lower left view*). Structures displayed as α-carbon traces using MASSHA (69).

component, non interacting species model, the major population (>95%) gave a sedimentation coefficient ($s_{20,w}$) of 3.17 ± 0.02 × 10^{-13} s^{-1} and a translational diffusion coefficient ($D_{20,w}$) of 6.5 ± 0.2 × 10^{-7} cm^2 s^{-1}. Assuming a partial specific volume of 0.721 ml/g (see "Experimental Procedures"), these data correspond to a particle of molecular mass 43 ± 2 kDa. Since this is close to the molecular mass of 48628 Da determined by mass spectrometry, or that calculated from the amino acid sequence (45550 Da, glycosylation not included) we conclude that rPCPE behaves in solution, for the most part, as a monomer.

While the determination of $s_{20,w}$ by analytical centrifugation is precise, that for $D_{20,w}$ is systematically overestimated even in the case of slight heterogeneity (72). Hence $D_{20,w}$ was also determined from the experimentally determined values of $s_{20,w}$ and molecular mass, determined by mass spectrometry, and the calculated partial specific volume (see "Experimental Procedures"). This gave a $D_{20,w}$ value of 5.7 × 10^{-7} cm^2 s^{-1}, corresponding to an hydrodynamic diameter D_h (*i.e.* that of a sphere with the same diffusion coefficient) of 74 Å. This result compares with calculated minimum D_h values of 48 and 56 Å for spherical non-hydrated and hydrated (0.4 g of water per gram of protein) PCPE, respectively. Since the observed D_h is greater, this indicates that rPCPE has an elongated structure. The ratio of the observed D_h to that calculated for spherical, hydrated rPCPE corresponds to a prolate or oblate ellipsoid with an axial ratio of at least 6.5.

Rotary Shadowing—rPCPE molecules were also observed directly by transmission electron microscopy after rotary shadowing. As shown in Fig. 3, a mixed population of particles was observed, about half of which were approximately globular in shape. The remainder were more rod-like in appearance with approximate dimensions 80 by 200 Å. A striking feature of most of these rod-like particles was their dumbbell-like structure consisting of two closely adjacent lobes (shown *circled* in Fig. 3).

Small Angle X-ray Scattering—To get further information on the shape of rPCPE in solution, the protein was analyzed by SAXS. The composite experimental scattering curve is shown in Fig. 4. Comparison of the forward scattering I (0) with that from bovine serum albumin gave an apparent molecular mass for rPCPE of 46 ± 2 kDa. This was consistent with the mass determined by mass spectrometry, or that calculated from protein sequence data, and confirmed that rPCPE was monomeric in solution.

The radius of gyration R_g of rPCPE, calculated by Guinier analysis of the data in Fig. 4, was 41 ± 3 Å. Using GNOM (63), R_g was found to be 43 ± 1 Å. These values correspond to an equivalent sphere of diameter at least 106 Å, which is larger than that calculated on the basis of the molecular mass, again showing rPCPE to be an extended molecule. To determine the maximum dimension of rPCPE from the SAXS data, the pair distribution function p(r) was also calculated using GNOM. As shown in Fig. 5, this revealed an asymmetric curve with a tail extending to a maximum particle length of ~150 Å. In addition, the program ORTOGNOM gave a maximum dimension of 140 ± 10 Å. Thus standard SAXS analysis confirmed the molecular mass as well as the elongated shape of the protein determined by analytical ultracentrifugation.

To determine the low resolution three-dimensional structure of rPCPE in solution, the *ab initio* programs DAMMIN (65), DALAI_GA (66), and GASBOR (67) were used as described in "Experimental Procedures." The modeling allowed us to neatly fit the experimental data with discrepancy factors χ (65) of about 0.6. A typical GASBOR fit is displayed in Fig. 4. With

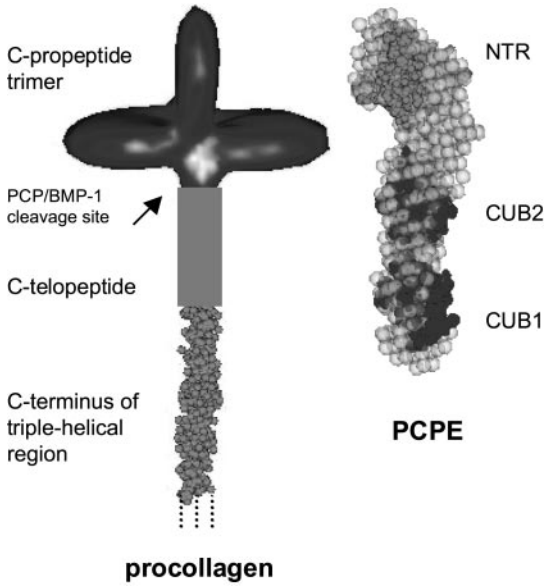

FIG. 9. **Structural comparison between rPCPE and the C-terminal region of the procollagen molecule.** Both structures are shown on the same scale. The CUB domains in rPCPE are sufficiently far apart to interact with both the C-propeptide trimer as well as with a putative site in the mature collagen domain of the procollagen molecule.

each program, results from at least ten separate runs were averaged to determine common structural features. The results are shown in Fig. 6, where each structure is represented by an array of beads, which serve to define the overall shape. All three modeling programs gave similar results, where rPCPE appeared as a bent, rod-like molecule of length ~150 Å. As the rod was somewhat flattened, the apparent thickness varied depending on the direction of view. End views showed a maximum width of ~60 Å, consistent with the highly elongated shape deduced by analytical ultracentrifugation. All structures showed evidence for both pointed and blunt ends to the rod, with a pronounced kink nearer the blunt end (Fig. 6).

Molecular Modeling—Three-dimensional atomic models of both CUB domains in rPCPE, as well as the NTR domain, were built on the basis of sequence homology (Fig. 7) with domains of known 3D structure. All three models, shown in Fig. 8, *A–C*, satisfied the constraints, exhibited good geometry (94, 96, and 95% in favorable regions of the Ramachandran plot for domains CUB1, CUB2, and NTR, respectively) and had low energies (−3933, −4602, and −4193 kcal/mol, respectively). The compactness of the models, all of which had the overall form of an oblate ellipsoid, was reasonable. Molecular dimensions (Fig. 8, *A–C*) calculated from the models were globally compatible with those estimated from the SAXS experiments.

As shown in Fig. 8*D*, when superimposed on the average structure generated using DAMMIN, these models fitted well into the overall shape, with room for additional contributions from regions of unknown structure, especially that of the 42-residue linker region between CUB2 and NTR. The best fit was obtained, by eye, with the pointed end corresponding to CUB1 and the blunt end corresponding to the somewhat larger NTR domain. The asymmetric shapes of the CUB domains fitted particularly well with the dimensions of the flattened rod-like structure of the entire PCPE molecule.

The proposed arrangement of domains was well accommodated within the low resolution shape, but the scattering computed from this model using the program CRYSOL (70) failed to fit the experimental data (not shown). The fit was significantly improved however by adding the missing portions of the structure, corresponding to N-terminal, C-terminal, and linker regions, using the program suite CREDO (71). The atomic positions of the domains arranged as in Fig. 8*D* were fixed, and additional native-like loops composed of dummy residues were generated to fit the experimental scattering data. Fig. 8*E* presents the best fit conformations of the missing fragments obtained in five independent runs, all of which, when included with the CUB and NTR domains, yielded good fits to the experimental data (minimum $\chi = 0.9$), as illustrated in Fig. 4. Although the added loops displayed somewhat different conformations in independent reconstructions, they were confined in space and permitted one to draw tentative volumes occupied by the missing portions of the structure.

DISCUSSION

Here we have shown that rPCPE is a rod-like molecule. The elongated shape deduced from analytical ultracentrifugation was confirmed by small angle x-ray scattering, which produced low-resolution models for the three-dimensional structure of the molecule. These models were then used as a basis to assemble the molecule from the predicted structures, built by homology modeling, of each of its CUB1, CUB2, and NTR domains.

The data obtained in solution are consistent with the images of rPCPE obtained by transmission electron microscopy after rotary shadowing, half of which revealed a rod-like structure of dimensions slightly greater than those determined by SAXS, while the remainder might correspond to end-on views of the molecule. The frequent observation of a dumbbell-like substructure by electron microscopy likely corresponds to the CUB and NTR regions connected by a thin linker region, consistent with the known susceptibility of this region to proteolytic attack (73). The lack of a dumbbell-like shape in the models derived from SAXS probably reflects differences between experimental techniques: SAXS gives a low resolution structure while rotary shadowing preferentially coats exposed parts of the structure with a metal layer up to 20 Å thick. The models shown in Fig. 8*E* include relatively thin and extended linkers between the CUB2 and NTR domains; these are consistent with the rotary shadowing images, though the linker region would not be as evident at low resolution. Thus the combination of the different experimental approaches provides a more complete picture of the overall structure of the PCPE molecule.

The molecular models generated for the CUB and NTR domains fitted well with the overall shape of rPCPE determined by *ab initio* modeling from the SAXS data. Furthermore, when the positions and orientations of the domains were manually fitted to the overall shape, and then the missing portions of the structure (terminal and linker regions) were modeled using CREDO, it was possible to obtain satisfactory agreement between observed and theoretical scattering curves. While this gives strong support to the *ab initio* modeling, it should be noted that fitting to the SAXS data does not permit verification of the high resolution structures shown in Fig. 8*E*. This must await independent structure determination by x-ray crystallography or NMR.

The elongated nature of the rPCPE molecule is surprising in view of the calculated isoelectric points of the CUB and NTR domains (pI values of 5.77, 4.33, and 9.21 for CUB1, CUB2, and NTR, respectively) which might be expected to favor CUB-NTR electrostatic interactions in a more compact structure. Instead, all three domains are in linear array. This is the first time that structural information has been obtained on a molecule containing two adjacent CUB domains. Because of the linear arrangement, interactions between CUB1 and CUB2 are probably limited to the external loops, and there is no evidence for stacking of CUB domains through β-sheet interactions as

observed in the seminal plasma glycoprotein PSP-I/PSP-II heterodimer (74).

We have recently shown that PCPE binds more tightly to the intact procollagen molecule than to its isolated C-propeptide trimer, probably due to the presence of additional binding sites within the mature collagen domain (38). Binding of PCPE to sites either side of the procollagen cleavage site might facilitate a conformational change leading to stimulation of PCP/BMP-1 activity. Such binding would involve the CUB domain region of PCPE, which is known to be essential for PCP/BMP-1 enhancing activity (10). The deduced structure of PCPE is consistent with such a mechanism, since comparison with the low resolution structure of the procollagen C-terminal region (75) (Fig. 9) reveals that the CUB domains are far enough apart to interact with both the C-propeptide and the collagen triple-helix. The future search for putative interaction sites on PCPE will be aided by the structural information obtained here.

Acknowledgments—We thank M. Becchi for help with the mass spectrometry analysis, E. Kessler for critical reading of the manuscript, and X. Robert for help with the computing.

REFERENCES

1. Bork, P., Downing, A. K., Kieffer, B., and Campbell, I. D. (1996) *Q. Rev. Biophys.* **29,** 119–167
2. Hohenester, E., and Engel, J. (2002) *Matrix Biol.* **21,** 115–128
3. Takahara, K., Kessler, E., Biniaminov, L., Brusel, M., Eddy, R. L., Janisait, S., Shows, T. B., and Greenspan, D. S. (1994) *J. Biol. Chem.* **269,** 26280–26285
4. Bányai, L., and Patthy, L. (1999) *Protein Sci.* **8,** 1636–1642
5. Takahara, K., Lyons, G. E., and Greenspan, D. S. (1994) *J. Biol. Chem.* **269,** 32572–32578
6. Kessler, E., Takahara, K., Biniaminov, L., Brusel, M., and Greenspan, D. S. (1996) *Science* **271,** 360–362
7. Li, S. W., Sieron, A. L., Fertala, A., Hojima, Y., Arnold, W. V., and Prockop, D. J. (1996) *Proc. Natl. Acad. Sci. U. S. A.* **93,** 5127–5130
8. Adar, R., Kessler, E., and Goldberg, B. (1986) *Collagen Rel. Res.* **6,** 267–277
9. Kessler, E., and Adar, R. (1989) *Eur. J. Biochem.* **186,** 115–121
10. Hulmes, D. J. S., Mould, A. P., and Kessler, E. (1997) *Matrix Biol.* **16,** 41–45
11. Prockop, D. J., Sieron, A. L., and Li, S.-W. (1998) *Matrix Biol.* **16,** 399–408
12. Imamura, Y., Steiglitz, B. M., and Greenspan, D. S. (1998) *J. Biol. Chem.* **273,** 27511–27517
13. Kessler, E., Fichard, A., Chanut-Delalande, H., Brusel, M., and Ruggiero, F. (2001) *J. Biol. Chem.* **276,** 27051–27057
14. Unsold, C., Pappano, W. N., Imamura, Y., Steiglitz, B. M., and Greenspan, D. S. (2002) *J. Biol. Chem.* **277,** 5596–5602
15. Rattenholl, A., Pappano, W. N., Koch, M., Keene, D. R., Kadler, K. E., Sasaki, T., Timpl, R., Burgeson, R. E., Greenspan, D. S., and Bruckner-Tuderman, L. (2002) *J. Biol. Chem.* **277,** 26372–26378
16. Uzel, M. I., Scott, I. C., Babakhaniou-Chase, H., Palamakumbura, A. H., Pappano, W. N., Hong, H. H., Greenspan, D. S., and Trackman, P. C. (2001) *J. Biol. Chem.* **276,** 22537–22543
17. Borel, A., Eichenberger, D., Farjanel, J., Kessler, E., Gleyzal, C., Hulmes, D. J. S., Sommer, P., and Font, B. (2001) *J. Biol. Chem.* **276,** 48944–48949
18. Scott, I. C., Imamura, Y., Pappano, W. N., Troedel, J. M., Recklies, A. D., Roughley, P. J., and Greenspan, D. S. (2000) *J. Biol. Chem.* **275,** 30504–30511
19. Amano, S., Scott, I. C., Takahara, K., Koch, M., Champliaud, M. F., Gerecke, D. R., Keene, D. R., Hudson, D. L., Nishiyama, T., Lee, S., Greenspan, D. S., and Burgeson, R. E. (2000) *J. Biol. Chem.* **275,** 22728–22735
20. Sasaki, T., Gohring, W., Mann, K., Brakebusch, C., Yamada, Y., Fassler, R., and Timpl, R. (2001) *J. Mol. Biol.* **314,** 751–763
21. Decline, F., and Rousselle, P. (2001) *J. Cell Sci.* **114,** 811–823
22. Garcia, A. J., Coffinier, C., Larrain, J., Oelgeschlager, M., and De Robertis, E. M. (2002) *Gene* (*Amst.*) **287,** 39–47
23. Scott, I. C., Blitz, I. L., Pappano, W. N., Imamura, Y., Clark, T. G., Steiglitz, B. M., Thomas, C. L., Maas, S. A., Takahara, K., Cho, K. W. Y., and Greenspan, D. S. (1999) *Dev. Biol.* **213,** 283–300
24. Xu, H., Acott, T. S., and Wirtz, M. K. (2000) *Genomics* **66,** 264–273
25. Zheng, X., Chung, D., Takayama, T. K., Majerus, E. M., Sadler, J. E., and Fujikawa, K. (2001) *J. Biol. Chem.* **276,** 41059–41063
26. Sim, R. B., and Laich, A. (2000) *Biochem. Soc. Trans.* **28,** 545–550
27. Arlaud, G. J., Gaboriaud, C., Thielens, N. M., Rossi, V., Bersch, B., Hernandez, J. F., and Fontecilla-Camps, J. C. (2001) *Immunol. Rev.* **180,** 136–145
28. Kitamoto, Y., Yuan, X., Wu, Q., Mccourt, D. W., and Sadler, J. E. (1994) *Proc. Natl. Acad. Sci. U. S. A.* **91,** 7588–7592
29. Hooper, J. D., Clements, J. A., Quigley, J. P., and Antalis, T. M. (2001) *J. Biol. Chem.* **276,** 857–860
30. Velasco, G., Cal, S., Quesada, V., Sanchez, L. M., and Lopez-Otin, C. (2002) *J. Biol. Chem.* **277,** 37637–37646
31. Romero, A., Romao, M. J., Varela, P. F., Kolln, I., Dias, J. M., Carvalho, A. L., Sanz, L., Topfer-Petersen, E., and Calvete, J. J. (1997) *Nat. Struct. Biol.* **4,** 783–788
32. Nentwich, H. A., Mustafa, Z., Rugg, M. S., Marsden, B. D., Cordell, M. R., Mahoney, D. J., Jenkins, S. C., Dowling, B., Fries, E., Milner, C. M., Loughlin, J., and Day, A. J. (2002) *J. Biol. Chem.* **277,** 15354–15362
33. Li, X., Ponten, A., Aase, K., Karlsson, L., Abramsson, A., Uutela, M., Backstrom, G., Hellstrom, M., Bostrom, H., Li, H., Soriano, P., Betsholtz, C., Heldin, C. H., Alitalo, K., Ostman, A., and Eriksson, U. (2000) *Nat. Cell Biol.* **2,** 302–309
34. Ligtenberg, T. J., Bikker, F. J., Groenink, J., Tornoe, I., Leth-Larsen, R., Veerman, E. C., Nieuw Amerongen, A. V., and Holmskov, U. (2001) *Biochem. J.* **359,** 243–248
35. Duke-Cohan, J. S., Tang, W., and Schlossman, S. F. (2000) *Adv. Exp. Med. Biol.* **477,** 173–185
36. Yammani, R. R., Seetharam, S., and Seetharam, B. (2001) *J. Biol. Chem.* **276,** 44777–44784
37. Gu, C., Limberg, B. J., Whitaker, G. B., Perman, B., Leahy, D. J., Rosenbaum, J. S., Ginty, D. D., and Kolodkin, A. L. (2002) *J. Biol. Chem.* **277,** 18069–18076
38. Ricard-Blum, S., Bernocco, S., Font, B., Moali, C., Eichenberger, D., Farjanel, J., Burchardt, E. R., van der Rest, M., Kessler, E., and Hulmes, D. J. S. (2002) *J. Biol. Chem.* **277,** 33864–33869
39. Thielens, N. M., Cseh, S., Thiel, S., Vorup-Jensen, T., Rossi, V., Jensenius, J. C., and Arlaud, G. J. (2001) *J. Immunol.* **166,** 5068–5077
40. Chen, C. B., and Wallis, R. (2001) *J. Biol. Chem.* **276,** 25894–25902
41. Yu, T. W., and Bargmann, C. I. (2001) *Nat. Neurosci.* **4,** (suppl.) 1169–1176
42. Chong, J. M., Uren, A., Rubin, J. S., and Speicher, D. W. (2002) *J. Biol. Chem.* **277,** 5134–5144
43. Trexler, M., Bányai, L., and Patthy, L. (2001) *Proc. Natl. Acad. Sci. U. S. A.* **98,** 3705–3709
44. Brew, K., Dinakarpandian, D., and Nagase, H. (2000) *Biochim. Biophys. Acta* **1477,** 267–283
45. Mott, J. D., Thomas, C. L., Rosenbach, M. T., Takahara, K., Greenspan, D. S., and Banda, M. J. (2000) *J. Biol. Chem.* **275,** 1384–1390
46. Masuda, M., Igarashi, H., Kano, M., and Yoshikura, H. (1998) *Cell Growth & Differ.* **9,** 381–391
47. Kanaki, T., Morisaki, N., Bujo, H., Takahashi, K., Ishii, I., and Saito, Y. (2000) *Biochem. Biophys. Res. Commun.* **270,** 1049–1054
48. Matsui, A., Yanase, M., Tomiya, T., Ikeda, H., Fujiwara, K., and Ogata, I. (2002) *Biochem. Biophys. Res. Commun.* **290,** 898–902
49. Sieron, A. L., Tretiakova, A., Jameson, B. A., Segall, M. L., Lund-Katz, S., Khan, M. T., Li, S. W., and Stöcker, W. (2000) *Biochemistry* **39,** 3231–3239
50. Garrigue-Antar, L., Hartigan, N., and Kadler, K. E. (2002) *J. Biol. Chem.* **277,** 43327–43334
51. Tuuttila, A., Morgunova, E., Bergmann, U., Lindqvist, Y., Maskos, K., Fernandez-Catalan, C., Bode, W., Tryggvason, K., and Schneider, G. (1998) *J. Mol. Biol.* **284,** 1133–1140
52. Fernandez-Catalan, C., Bode, W., Huber, R., Turk, D., Calvete, J. J., Lichte, A., Tschesche, H., and Maskos, K. (1998) *EMBO J.* **17,** 5238–5248
53. Kohfeldt, E., Maurer, P., Vannahme, C., and Timpl, R. (1997) *FEBS Lett.* **414,** 557–561
54. Moschcovich, L., Bernocco, S., Font, B., Rivkin, H., Eichenberger, D., Chejanovsky, N., Hulmes, D. J. S., and Kessler, E. (2001) *Eur. J. Biochem.* **268,** 2991–2996
55. Schuck, P. (1998) *Biophys. J.* **75,** 1503–1512
56. Schuck, P., and Demeler, B. (1999) *Biophys. J.* **76,** 2288–2296
57. Mould, A. P., Holmes, D. F., Kadler, K. E., and Chapman, J. A. (1985) *J. Ultrastruct. Res.* **91,** 66–76
58. Koch, M. H. J., and Bordas, J. (1983) *Nucl. Instrum. Methods* **208,** 461–469
59. Boulin, C., Kempf, R., Koch, M. H. J., and McLaughlin, S. M. (1986) *Nucl. Instrum. Methods* **249,** 399–407
60. Boulin, C., Kempf, R., Gabriel, A., and Koch, M. H. J. (1988) *Nucl. Instrum. Methods* **269,** 312–320
61. Gabriel, A., and Dauvergne, F. (1982) *Nucl. Instrum. Methods* **201,** 223–224
62. Feigin, L. A., and Svergun, D. I. (1987) *Structure Analysis by Small Angle X-ray and Neutron Scattering*, Plenum Press, New York
63. Svergun, D. I. (1992) *J. Appl. Crystallogr.* **25,** 495–503
64. Svergun, D. I. (1993) *J. Appl. Crystallogr.* **26,** 258–267
65. Svergun, D. I. (1999) *Biophys. J.* **76,** 2879–2886
66. Chacon, P., Diaz, J. F., Moran, F., and Andreu, J. M. (2000) *J. Mol. Biol.* **299,** 1289–1302
67. Svergun, D. I., Petoukhov, M. V., and Koch, M. H. (2001) *Biophys. J.* **80,** 2946–2953
68. Combet, C., Jambon, M., Deleage, G., and Geourjon, C. (2002) *Bioinformatics* **18,** 213–214
69. Konarev, P. V., Petoukhov, M. V., and Svergun, D. I. (2001) *J. Appl. Crystallogr.* **34,** 527–532
70. Svergun, D. I., Barberato, C., and Koch, M. H. J. (1995) *J. Appl. Crystallogr.* **28,** 768–773
71. Petoukhov, M. V., Eady, N. A. J., Brown, K. A., and Svergun, D. I. (2002) *Biophys. J.* **83,** 3113–3125
72. Philo, J. S. (1997) *Biophys. J.* **72,** 435–444
73. Kessler, E., Mould, A. P., and Hulmes, D. J. S. (1990) *Biochem. Biophys. Res. Commun.* **173,** 81–86
74. Varela, P. F., Romero, A., Sanz, L., Romao, M. J., Topfer-Petersen, E., and Calvete, J. J. (1997) *J. Mol. Biol.* **274,** 635–649
75. Bernocco, S., Finet, S., Ebel, C., Eichenberger, D., Mazzorana, M., Farjanel, J., and Hulmes, D. J. S. (2001) *J. Biol. Chem.* **276,** 48930–48936
76. Kozin, M. B., Volkov, V. V., and Svergun, D. I. (1997) *J. Appl. Crystallogr.* **30,** 811–815